

Article

Buckling Defect Optimization of Constrained Ring Rolling of Thin-Walled Conical Rings with Inner High Ribs Combining Response Surface Method with FEM

Wei Feng ^{1,2,3,*}  and Peng Zhao ¹

¹ School of Materials Science and Engineering, Wuhan University of Technology, Wuhan 430070, China; 317328@whut.edu.cn

² Hubei Engineering Research Center for Green Precision Material Forming, Wuhan 430070, China

³ Hubei Key Laboratory of Advanced Technology for Automotive Components, Wuhan University of Technology, Wuhan 430070, China

* Correspondence: fengwei@whut.edu.cn

Abstract: A buckling defect will appear on the outer surface of the deformed ring during the constrained ring rolling (CRR) of an aluminum alloy thin-wall conical ring with inner high ribs (AATWCRIHR) if the geometrical dimension of the ribs does not match the wall thickness. To avoid the buckling defect, a quantitative method for characterizing the degree of the buckling defect is proposed using the area of the buckling profile. Then, an orthogonal experimental scheme was designed, taking the width of the middle rib, thickness of wall, and height of the middle rib as the design variables and defining the area of the buckling profile as the optimization objective. Subsequently, a quadratic polynomial response surface model was established by combining the optimization algorithm with the finite element method (FEM), and the geometrical dimension of the middle ribs of the deformed AATWCRIHR is optimized. Moreover, the optimal parameter combination to minimize the area of the buckling profile is obtained and verified using FE simulation. The results show that the AATWCRIHR after optimization does not generate the buckling defect during constrained ring rolling, and it is proven that the quantitative buckling defect representation method and the optimization design method based on the response surface model and the finite element simulation results are feasible for the constrained ring-rolling process of the AATWCRIHR.

Keywords: aluminum alloy thin-wall conical ring with inner high ribs; constrained ring rolling; buckling defect optimization; FE simulation; response surface method



Citation: Feng, W.; Zhao, P. Buckling Defect Optimization of Constrained Ring Rolling of Thin-Walled Conical Rings with Inner High Ribs Combining Response Surface Method with FEM.

Metals **2024**, *14*, 378. <https://doi.org/10.3390/met14040378>

Academic Editor: Giovanni Meneghetti

Received: 28 February 2024

Revised: 20 March 2024

Accepted: 21 March 2024

Published: 24 March 2024



Copyright: © 2024 by the authors. Licensee MDPI, Basel, Switzerland. This article is an open access article distributed under the terms and conditions of the Creative Commons Attribution (CC BY) license (<https://creativecommons.org/licenses/by/4.0/>).

1. Introduction

Thin-wall ring parts with high ribs made of aluminum alloy are the key components of aerospace equipment. Due to the structural characteristics of a thin wall and high ribs, the material characteristics of a low-density aluminum alloy thin-wall conical ring with inner high ribs (AATWCRIHR) have the advantages of light weight, high strength, and strong carrying capacity [1], and have been widely used in aerospace equipment such as rockets and high-speed aircraft [2].

At present, the AATWCRIHR is manufactured using traditional machining technology and precision-casting methods, which is of low material utilization rate and low strength, and, thus, it is difficult to meet the higher performance requirement of aerospace equipment in the new era. The integral plastic-forming manufacturing method is an effective way to achieve lightweight components and improve their performance [3]. The ring-rolling technology is a plastic-forming method for manufacturing the ring part by reducing the thickness and height of the parts under the action of the local compression of the material through the rolling roll [4]. Kopp et al. developed rolls composed of several different-shaped rings to form a strip with a variable thickness profile [5]. Clever et al. proposed a

new ring-rolling process consisting of six rolls, which is ideal for the production of special-shaped rings without diameter expansion, and analyzed and predicted the collapse defect that occurs during the forming process using 22 experiments on lead rings, also providing the suggestion of optimal thickness reduction per pass to avoid collapse [6]. Lohmar et al. studied the influence of the number of guide rolls on the temperature distribution and evolution of the formed parts during the radial ring-rolling process, and found that thin rings were more affected by guide rolls than thick rings [7]. Li et al. developed the calculation model for the bending moment and normal stress at different sections of the deformed ring during the radial-axial ring-rolling process with four guide rolls, and established the criterion of plastic instability and obtained the mathematical model of the critical guide force of plastic instability [8]. Yeom et al. combined finite element simulation and the flow instability map to optimize the heating temperature and the feed speed of the rolling roll during the ring-rolling process, and obtained a defect-free ring part [9]. Liang et al. showed the deformation mechanism of the deformed ring with the groove-section profile in the ring-rolling process, and determined the critical thickness of the billet with a good forming effect based on the proposed pulling model [10]. On the basis of the basic principle of the rolling process, Han et al. proposed a radial envelope-forming process for manufacturing cylindrical rings with cross ribs, and its feasibility was verified by simulation and experiment [11].

As one of the precision plastic-forming methods, the constrained ring-rolling (CRR) process uses the external constraint roll to restrict the radial flow of the material, and the upper and lower cover plates to restrict the axial flow of the material, which makes the metal flow along the radial direction by reducing the wall thickness of the ring billet while the outer diameter of the ring billet remains unchanged and is beneficial to the growth of the high ribs, as shown in Figure 1. The constrained ring-rolling (CRR) process has the advantages of high machining accuracy, small forming load, good performance of forming parts, and so on, and has great potential in forming thin-walled rings with high ribs [12–14]. There are still some problems such as the insufficient rib filling and buckling defect in the outer wall during the constrained ring-rolling process of the AATWCRIHR, which will affect the application of the deformed component. As a result, some measures must be taken to avoid these problems in order to guarantee the forming quality. Aiming at all kinds of problems in the forming process, many scholars currently combine finite element simulation and various optimization algorithms to find the most suitable process design scheme with a lower cost and higher forming quality [15].

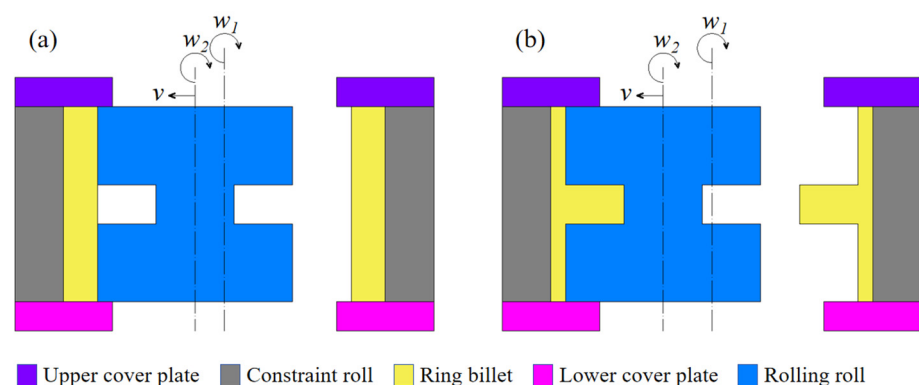


Figure 1. Principle of CRR: (a) beginning of CRR; and (b) end of CRR. v , w_1 and w_2 are the radial feeding speed of rolling roll, the angular velocities of constraint roll and rolling roll, respectively.

Zhao et al. has proposed an optimization algorithm for the design of preforms and promoted the application of optimization algorithms in preforms [16]. Fourment et al. combines finite element simulation with an optimization algorithm, and can successfully solve problems such as the flow uniformity of metal materials by using different objective functions [17]. Kusiak et al. introduced gradient-free technology into the design of preform dies,

which improves the efficiency of the preform optimization design to a certain extent [18]. Box and Wilson et al. combined mathematical methods with statistical methods to propose the response surface method (RSM), which greatly improved the computational efficiency and has been widely used in the field of plastic forming [19]. Gheyserian et al. combined the finite element simulation method with the response surface method, taking the surface roughness, maximum thickness change, forming time, and forming force as optimization objectives, and obtained the best process parameters in the incremental sheet metal forming process [20]. Vishal et al. combined response surface tables with an analysis of variance to determine the greatest influence on the part formability and surface roughness in the single point incremental forming process of aluminum alloys [21]. Pan et al. used the response surface method to optimize the friction coefficient, pressure rate, and fillet radius of the die in the process of hydromechanical deep drawing, and obtained the best conditions to meet the maximum thinning rate. The reliability of the optimized results was verified by process experiments [22]. Li et al. used the thickness of the patched blank, the distance between the welding spot, the external contour of the patched blank, and the number of welding spots as optimization variables, and analyzed the influence of the distribution of welding spots on the quality of welding. The optimized welding spot arrangement method was used to carry out the process experiment, and the parts with a high forming quality were obtained [23]. Combining RSM and FEM, Hu et al. studied the effects of the friction factor, the fillet radius of the cavity, and the diameter of the rolling roll on the heights of the longitudinal and transverse ribs and obtained the optimal process combination [24]. Hu et al. reviewed various optimization methods of metal rolling to discuss the relationship between the process parameters and the optimization objectives in the metal-rolling process [25]. Based on the finite element method and the Taguchi method, Feng et al. optimized the component damage value, maximum forging force, and mold-filling quality during the warm-forging process of the spiral gear, and the optimal parameter combination was obtained through signal-to-noise ratio analysis and variance analysis; moreover, the actual experimental results are in good agreement with the predicted values. The feasibility of the optimization method is verified [26,27]. Francy et al. optimized the extrusion parameters based on the Taguchi method for aluminum alloy cold extrusion forming, and verified the theoretical results, and concluded that the extrusion ratio is the most significant factor affecting the extrusion pressure [28]. Based on finite element numerical simulation, Li et al. took the extrusion pressure and velocity field standard deviation as optimization objectives to study the extrusion deformation behavior of 2195Al-Li alloy, and obtained the best combination of extrusion process parameters [29]. Luo et al. has designed an orthogonal experiment to study the warping problem in the injection molding process of automotive plastic wings, and established a BP neural network by a genetic algorithm for global optimization, and obtained the best parameter combination of the plastic wing injection molding process [30]. Hosseini et al. used the Taguchi method to optimize the critical thickness of aluminum alloy during forward extrusion and obtained the optimal level of waste minimization [31].

In this paper, the buckling defect area was used to characterize the degree of the buckling defect quantitatively and the main factors affecting the degree of the buckling defect were analyzed. Orthogonal test tables were designed and finite element numerical simulation was carried out and a response surface model was established by defining the height, width, and thickness of the ribs as the design variables and the buckling defect area as the optimization objective. Through the combination of the response surface method with finite element simulation, the influence of different parameters on the degree of the defect is analyzed and the optimal parameter combination without the buckling defect is obtained.

2. Optimization Method

2.1. Establishment of Finite Element Model of Constrained Ring Rolling of AATWCRIHR

In this paper, an AATWCRIHR with three ribs is taken as the research object. Figure 2 shows the main structural features and the main dimensions of the AATWCRIHR. The

AATWCRIHR has an outer diameter of 440 mm at the large end, a cone angle of 7° , and an axial height of 224 mm. Three horizontal high ribs are arranged along the inner wall of the conical ring. The three ribs are of different heights and widths, and their values are as follows: the thickness of wall t is 5 mm, the widths of the three ribs b_1 , b_2 , and b_3 are 19 mm, 40 mm, 19 mm, respectively, and the heights of the three ribs h_1 , h_2 , and h_3 are 27 mm, 51 mm, and 38 mm, respectively.

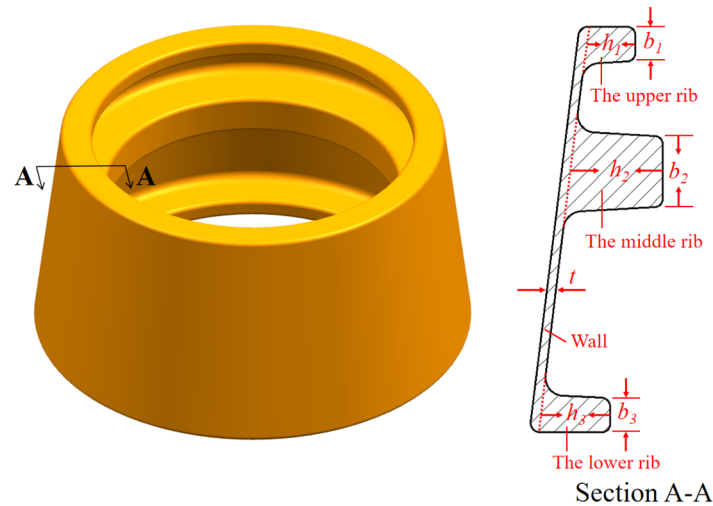


Figure 2. Aluminum alloy thin-walled conical ring with inner high ribs.

The DEFORM-3D v13.0 software was used to simulate the constrained rolling process of the thin-walled conical ring with high ribs. Based on the principle of the constrained ring-rolling process, a finite element model was established, as shown in Figure 3. The conical ring billet has the same outer diameter of 440 mm at the large end and a cone angle of 7° as the AATWCRIHR, and a wall thickness of 17 mm and an axial height of 224 mm, according to the principle of equal volume. The outer surface profile of the rolling roll is consistent with the inner surface profile of the AATWCRIHR, and the inner surface profile of the constraint roll is consistent with the outer surface profile of the AATWCRIHR. Before the CRR process begins, the conical ring billet is in close contact with the rolling roll and the constraint roll, respectively. During the CRR process, the rolling roll carries on the radial feed motion and exerts radial force on the conical ring billet, and causes local deformation of the conical ring billet. The constraint roll rotates actively around the central axis and drives the conical ring billet to rotate at the same angular velocity under the action of friction. Under the radial extrusion of the rolling roll and the radial constraint of the constraint roll, the metal billet flows along the radial direction to promote the formation of the three ribs. The conical ring billet is made of 2219 aluminum alloy and the initial deformation temperature is set to 450°C . The material model comes from the material library of the DEFORM-3D software and the main mechanical and thermodynamic properties are shown in the Table 1, and the flow stress–strain curves at different strain rates are shown in Figure 4. All molds are made of H13 steel with an initial preheating temperature of 300°C . The conical ring billet and all molds are defined as plastic body and rigid body, respectively. The radial feed speed of the rolling roll is set to 0.25 mm/s, and the rotation angular speed of the constraint roll is set to $2\pi\text{rad/s}$. The constant shear type is defined and the friction coefficient between the billet, rolling roll, and constraint roll is set to 0.3, and the heat transfer coefficient is set to $11\text{ N/s/mm}^\circ\text{C}$.

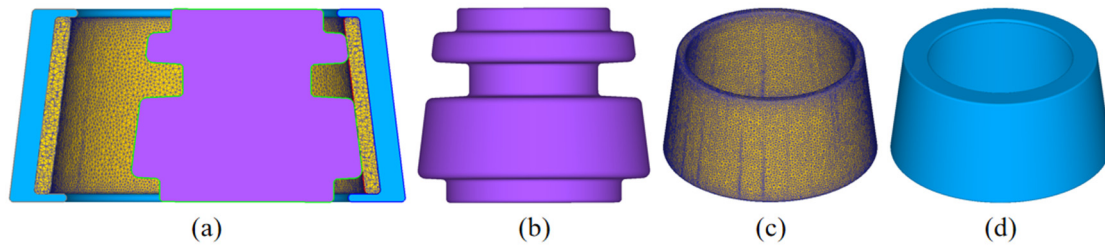


Figure 3. Finite element model of CRR: (a) section view of FE model; (b) rolling roll; (c) conical ring billet; and (d) constraint roll.

Table 1. The main mechanical and thermodynamic properties of 2219 aluminum alloy.

Parameter	Tensile Strength (MPa)	Yield Strength (MPa)	Elastic Modulus (GPa)	Poisson's Ratio	Thermal Conductivity ($W \times m^{-1} \times K^{-1}$)	Specific Heat Capacity ($J \times Kg^{-1} K^{-1}$)
Value	175	75	73	0.33	180.2	901

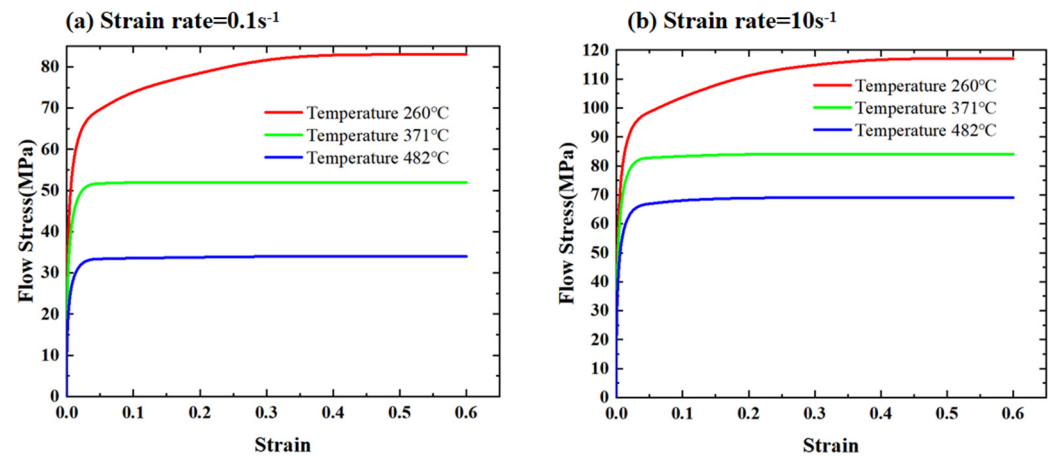


Figure 4. Flow stress-strain curves at different strain rates of 2219 aluminum ally: (a) strain rate of $0.1 s^{-1}$; and (b) strain rate of $10 s^{-1}$.

2.2. Evaluation Criteria of Buckling Defect

The result of the finite element simulation of the rolling process is shown in Figure 5. It can be seen that the conical ring is in good shape without an instability defect, and the inner horizontal ribs gradually increases with the increase in rolling time, and the filling effects of the three ribs is good. However, the outer surface of the middle rib began to show the circular buckling defect phenomenon in the middle stage of the rolling process, and the buckling degree increased gradually with the increase in rolling time.

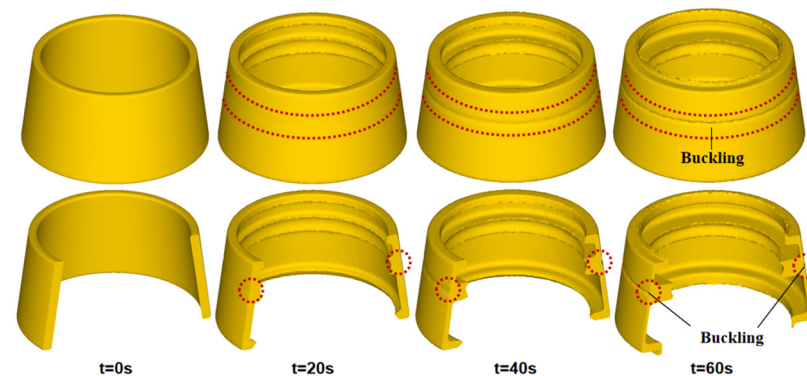


Figure 5. FE simulation result of CRR for AATWCRIHR.

In order to quantitatively analyze the degree of the buckling defect and to study the influence factor of buckling defect formation, a calculation method is proposed by measuring the area of the buckling profile under different rolling times. When the buckling defect appears on the outer surface of the part, a random axial section of the deformed conical ring is obtained and the profile of the buckling defect can be shown based on the simulation results of the CRR process by the finite element software, as shown in Figure 6a. Dozens of points are taken along the buckling profile, the location information of these points is extracted, and the boundary curves l_2 and l_3 of the buckling contour are, respectively, drawn, as shown in Figure 6b. The straight line l_1 is the initial outer surface profile of the conical ring billet at the beginning of the rolling process. The area enclosed by straight lines l_1 and boundary curve l_2 and l_3 is used to quantitatively represent the degree of the buckling defect. In Figure 6b, point B is the point with the greatest degree of buckling, and point A and point C are the junction points between the buckling zone and the non-buckling zone.

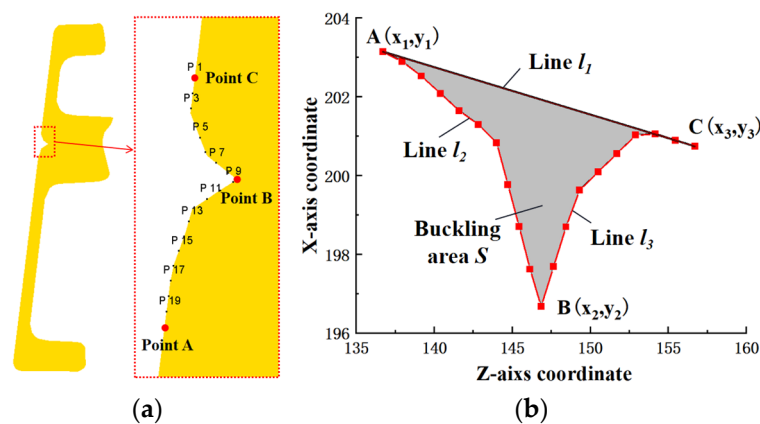


Figure 6. Calculation method degree of buckling defect: (a) the data extraction points; and (b) schematic diagram of buckling area S calculation.

The straight line l_1 can be expressed by Equation (1):

$$y_1 = ax + c[x \in x_1, x_3] \tag{1}$$

where a and c are constants, and x_1 and x_3 are X -axis co-ordinates of point A and C , respectively.

The expression of the boundary curve l_2 and l_3 are shown in Equations (2) and (3), respectively.

$$y_2 = a_1x^2 + b_1x + c_1[x \in x_1, x_2] \tag{2}$$

$$y_3 = a_2x^2 + b_2x + c_2[x \in x_2, x_3] \tag{3}$$

where $a_1, a_2, b_1, b_2, c_1,$ and c_2 are constants, and x_2 is the X -axis co-ordinate of point B .

The expression of the area of buckling profile S can be given in Equation (4) by the integral method.

$$S = \int_{x_1}^{x_3} l_1 dx - \int_{x_1}^{x_2} l_2 dx - \int_{x_2}^{x_3} l_3 dx [x \in (x_1, x_3)] \tag{4}$$

Constants $a, c, a_1, a_2, b_1, b_2, c_1,$ and c_2 of Equations (1)–(3) can be determined according to the simulation results. Then, the area of buckling profile S can be calculated using Equation (4), and the degree of the buckling defect can be analyzed quantitatively, which will facilitate the subsequent buckling defect optimization; thus, the forming quality of the AATWCRIHR can be improved.

2.3. Determination of Experimental Scheme

Based on the above results of the finite element simulation, it is found that the buckling defect is consistently located on the back of the middle rib throughout the CRR process; in addition, the height and the width of the middle rib is the largest and the material flow behavior is the most complicated in the CRR process. Moreover, the growth of the high ribs is achieved by reducing the wall thickness. Therefore, it is preliminarily determined that the width and height of the middle rib and the thickness of the wall are three factors affecting the degree of buckling when other deformation process conditions are certain, and present them using symbols of A, B, C. In order to find the optimal design scheme of geometric dimensioning for the AATWCRIHR without a buckling defect or with the smallest degree of the buckling defect, three factors, namely, the width of the middle rib b_2 , the thickness of the wall t of the conical ring billet, and the height of the middle rib h_2 , were taken as independent design variables, four levels were selected for each factor, and the area of buckling profile S was selected as the optimized objective function. The smaller the S is, the less likely the deformed AATWCRIHR is to generate buckling defects in constrained ring rolling, and the better the manufactured AATWCRIHR quality will be. An orthogonal experimental table with three factors and four levels was designed, as shown in Table 2.

Table 2. Influencing factors and levels.

Symbol	Factors	Level 1	Level 2	Level 3	Level 4
A	Width of rib/ b_2 (mm)	24	30	35	40
B	Thickness of wall/ t (mm)	3	4	5	6
C	Height of rib/ h_2 (mm)	41	46	51	56

3. Results and Analysis

3.1. Orthogonal Experimental Analysis

Sixteen groups of experiments are designed according to the orthogonal experiment table selected, and the finite element simulation was carried out for each group of experiments. The buckling defect contour information was extracted on the basis of the finite element results of each group, and the area of buckling profile S was calculated by Equation (4). The orthogonal experimental data and calculation results are shown in Table 3. K_1 , K_2 , K_3 , and K_4 are the average value of the experimental data of each factor at different levels, respectively, and Range R_s is the difference between the maximum and the minimum values of K_1 , K_2 , K_3 , and K_4 , and can be used to judge the merits and demerits of each factor. The larger the value of R_s is, the greater the influence of the factor on the objective function S is. It can be seen from Table 3 that factor A has the largest R_s value, factor B follows, and factor C has the smallest R_s value. Therefore, the most important factor affecting the degree of the buckling defect is the width of the middle rib, the thickness of the wall is a secondary factor, and the height of the middle rib has a relatively small influence on the degree of the buckling defect.

Table 3. Orthogonal experimental results.

Experiment NO.	A (mm)	B (mm)	C (mm)	S (mm ²)
1	24	3	41	0.58
2	24	4	56	0.85
3	24	5	51	0.87
4	24	6	46	0.44
5	30	3	46	0.57
6	30	4	56	0.83
7	30	5	51	0.82
8	30	6	41	0.83
9	35	3	51	11.35

Table 3. Cont.

Experiment NO.	A (mm)	B (mm)	C (mm)	S (mm ²)
10	35	4	41	10.85
11	35	5	46	7.75
12	35	6	56	3.92
13	40	3	56	26.30
14	40	4	46	25.32
15	40	5	41	22.42
16	40	6	51	12.75
K ₁	0.68	9.70	8.67	
K ₂	0.76	9.46	8.52	
K ₃	8.47	7.69	6.44	
K ₄	21.70	4.48	7.98	
Range R _s	−21.01	−5.21	−2.23	

3.2. Orthogonal Experimental Level Analysis

According to the orthogonal experimental data and the value of K_1 , K_2 , K_3 , and K_4 shown in Table 3, the variation graph of the average value of buckling area S at different levels for each factor can be derived, as shown in Figure 7. As can be seen from the figure, when the width of the middle rib is 24 mm, the wall thickness is 6 mm, and the height of the middle rib is 51 mm, the area of buckling profile S is the smallest; that is, the degree of the buckling defect on the back of the middle rib is the lowest. Therefore, the optimal factor level combination is $A_1B_4C_3$. When the width of the middle rib is 40 mm, the wall thickness is 3 mm, and the height of the middle rib is 41 mm, the buckling area is the largest, and the degree of the buckling defect is at the worst level.

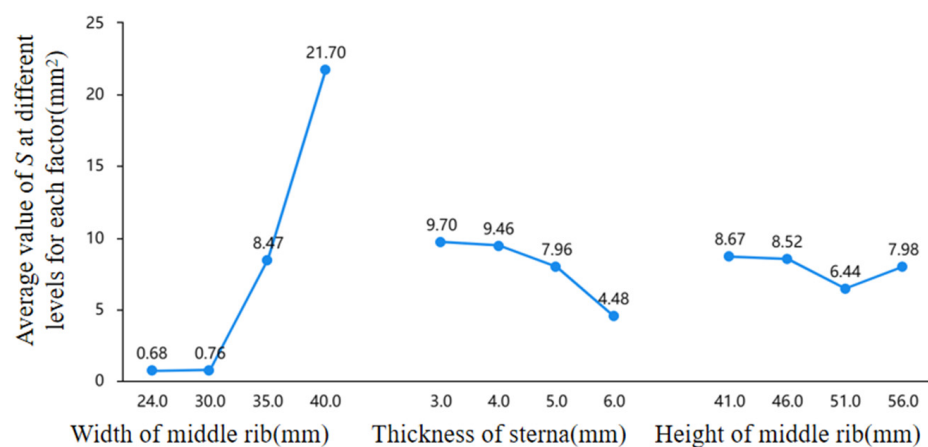


Figure 7. The variation graph of the average value of buckling area S at different levels for each factor.

3.3. Establishment of Response Surface Model

The response surface method (RSM) is an approximate method to predict and optimize the response value by fitting the experiment results of different experimental schemes to build a response surface. In this paper, the second-order polynomial response surface model is chosen as an approximate model to predict the relationship between objective function S and the design variables in the constrained ring rolling of an AATWCRIHR by FE simulation.

Based on the simulation results shown in Table 3, the regression analysis method was adopted to establish a regression model between the area of the buckling profile S and the width of the middle rib, the wall thickness, and the height of the middle rib, as shown in Equation (5). This model can be used to predict the degree of the buckling defect during

the constrained rolling of the thin-walled conical rings with inner transverse ribs under different widths and heights of the middle rib and the thickness wall.

$$S = 90.888 - 5.5069 \times A + 14.4967 \times B - 2.0632 \times C - 0.315 \times A \times B + 0.0035 \times A \times C + 0.0019 \times B \times C + 0.1262 \times A^2 - 0.9025 \times B^2 + 0.0185 \times C^2 \quad (5)$$

3.4. Analysis of Variance (ANOVA)

An analysis of variance (ANOVA) was used to analyze the significance of the primary terms, interaction terms, and square terms in the regression model, and the results were shown in Table 4. As can be seen from Table 4, the F-value of the model is 104.82, and the p -value is <0.0001 , indicating that the regression model has reached a very significant level and the model fitting accuracy is high. In addition, the correlation coefficient R^2 , the modified coefficient of determination R_{pred}^2 and the model prediction coefficient R_{adj}^2 are also commonly used to test the degree of fit of the regression models. Generally speaking, the larger the R^2 is, the higher and closer the values of R_{pred}^2 and R_{adj}^2 are, the higher the degree of fitting is, and the more accurate the regression model is. As can be seen from Table 4, the fitting degree of the model reaches 99.37%, and the values of R_{pred}^2 and R_{adj}^2 are 0.9842 and 0.9355, respectively, which are very close, indicating that the regression model has a high accuracy and can better describe the relationship between the objective function S and the design variables A , B , and C .

Table 4. Analysis of variance.

Source	Sum of Squares	DOF	Mean Square	F-Value	p -Value	Degree of Significance
Model	1316.65	9	146.29	104.82	<0.0001	significant
A	926.77	1	926.77	664.04	<0.0001	
B	47.21	1	47.21	33.83	0.0011	
C	10.96	1	10.96	7.85	0.0311	
AB	38.32	1	38.32	27.46	0.0019	
AC	0.073	1	0.073	0.052	0.8269	
BC	1.206×10^{-3}	1	1.206×10^{-3}	8.640×10^{-4}	0.9775	
A^2	211.28	1	211.28	151.38	<0.0001	
B^2	4.57	1	4.57	3.27	0.1205	
C^2	3.40	1	3.40	2.44	0.1695	
Residual error	8.37	6	1.40			
Correlation coefficient R^2	0.9937	Modified coefficient of determination R_{adj}^2	0.9842	Model prediction coefficient R_{pred}^2	0.9355	S/N Ratio
						28.303

The larger the F-value and the smaller the p -value are, the more significant the correlation coefficient is. From the F-value and p -value of each factor in Table 4, it can be seen that the p -value of the primary term A and the square term $A^2 < 0.0001$ reached a very significant level, indicating that factors A and A^2 have a very significant effect on the degree of the buckling defect. The P -values of the primary terms B and C and the interaction term $AB < 0.05$, which reached a significant level, indicate that factors B , C , and AB had a significant effect on the degree of buckling.

3.5. RSM Analysis

In order to directly analyze the influence of design variables A , B , and C on the response variables S in the constrained rolling process of the AATWCRIHR, the relationship between significant variables A and B and the response variables S was described by using a three-dimensional surface diagram, as shown in Figure 8. As can be seen from Figure 8, when the width of the middle rib is larger, ranging from 32 to 40 mm, the buckling area is also larger, so the degree of the buckling defect becomes more significant with the decrease

in wall thickness. When the width of the middle rib is smaller, ranging from 24 mm to 32 mm, the thickness of the wall has little influence on the buckling defect, and the buckling area is small and the degree of the buckling defect is light.

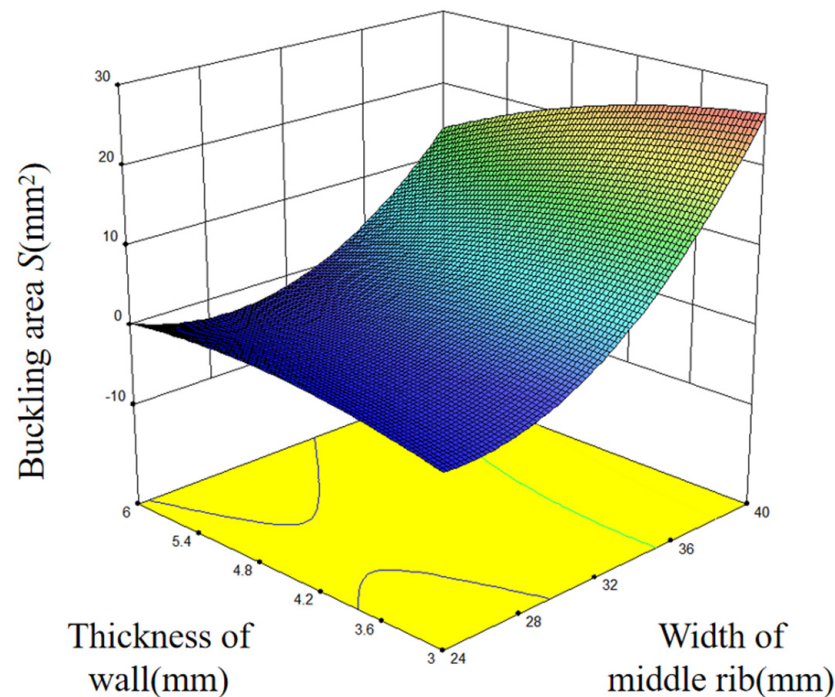


Figure 8. 3D response surface diagram of significant variables A and B and buckling area S.

4. Verification Model

In order to verify the accuracy of the response surface optimization results for the constrained ring rolling process of the AATWCRIHR, the DEFORM-3D software was used to simulate the optimal level; namely, the width of the middle rib is 24 mm, the thickness of the wall is 6 mm, and the height of the middle rib is 51 mm. The simulation results after optimization were compared with the simulation results before optimization. The optimized simulation results are shown in Figure 9. It can be seen from Figure 9 that no obvious annular buckling defect occurs in the outer surface of the formed parts from the beginning to the end of the rolling process; moreover, the three ribs are fully filled and have a very good forming quality according to the section profile diagram of the AATWCRIHR. The buckling area at the back of the middle rib before and after optimization was calculated, as shown in Figure 10. As can be seen from the figure, the buckling area after optimization is almost constant and its value is about zero from the beginning stage to the end stage of rolling, which indicates the degree of the buckling defect on the back of the middle rib is very low, so it can be considered that there will be no buckling defect on the outer surface of the conical ring when the width of the middle rib is 24 mm, the thickness of the wall is 6 mm, and the height of the middle rib is 51 mm. By comparing the simulation results and prediction results before and after optimization, it is proven that the quantitative buckling defect representation method and the optimization design scheme based on the response surface method are feasible for the constrained ring rolling process of the AATWCRIHR.

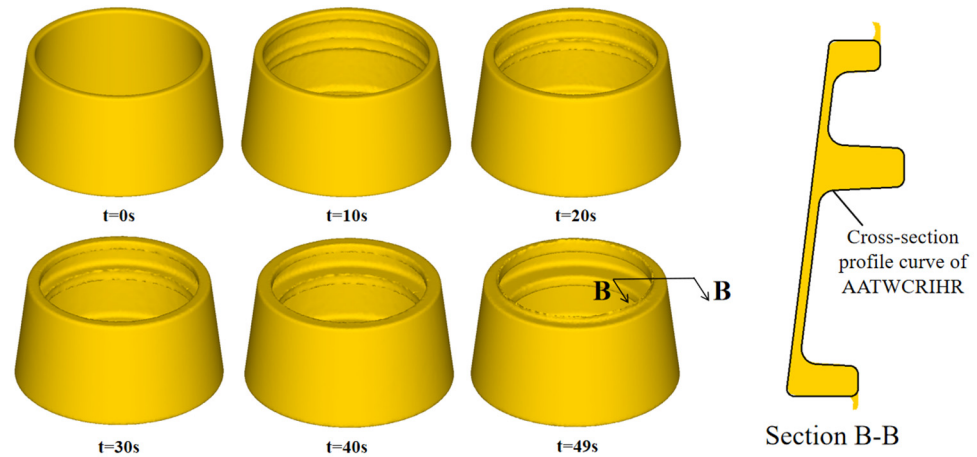


Figure 9. Optimized simulation results.

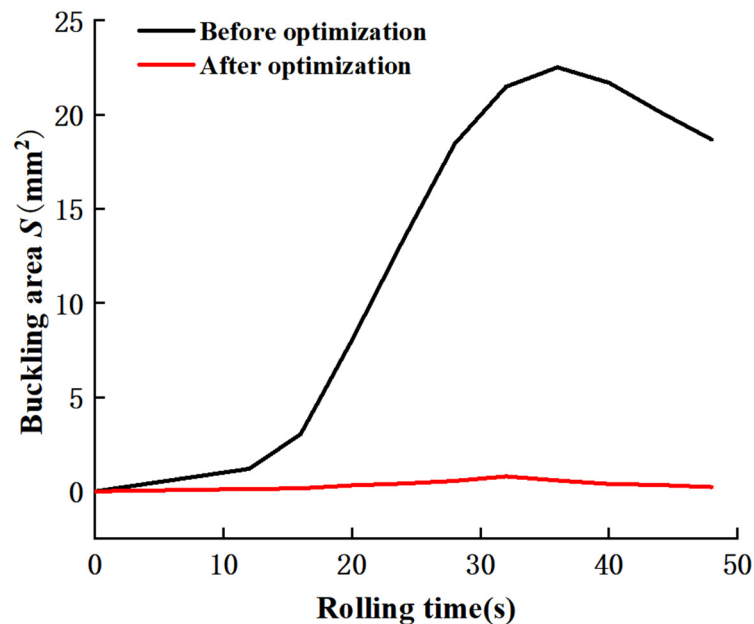


Figure 10. Buckling area before and after optimization.

5. Conclusions

Based on the response surface method and the finite element simulation results, the geometric dimensions of the middle rib and the wall thickness were optimized to minimize the degree of the buckling defect in the CRR process of the AATWCRIHR. According to the range analysis, level analysis, variance analysis, and response surface analysis, the following conclusions are obtained:

1. The degree of influence on the buckling defect is the width of the middle rib, the wall thickness, and the height of the middle rib, in that order.
2. The buckling area is the smallest and the degree of the buckling defect on the back of the middle rib is the lowest when the width of the middle rib is 24 mm, the wall thickness is 6 mm, and the height of the middle rib is 51 mm.
3. When the width of the middle rib is larger, the degree of the buckling defect becomes more significant with the decrease in wall thickness. When the width of the middle rib is smaller, the thickness of the wall has little influence on the buckling defect, and the degree of the buckling defect is light.
4. The quantitative representation of the buckling defect proposed using the buckling profile S is feasible, and the response surface model can predict the degree of the

buckling defect at a given geometry dimension of the middle rib and the wall thickness of the conical ring billet by verification.

However, the above research mainly focused on the effect of the width of the middle rib, the wall thickness, and the height of the middle rib of the AATWCRIHR on the buckling defect. But forming process parameters such as the billet deformation temperature, the radial feed speed of the rolling roll, the rotation angular speed of the constraint roll, and so on also influence the forming quality of the AATWCRIHR in the CRR process, so some more in-depth research about the material deformation law and the effect law of process parameters on the forming quality will continue to be performed in our future work.

Author Contributions: P.Z. and W.F. resources; W.F. data curation; P.Z. writing—original draft preparation; P.Z. writing—review and editing; W.F. and P.Z. visualization; P.Z. supervision; W.F. project administration; W.F. funding acquisition. All authors have read and agreed to the published version of the manuscript.

Funding: This research was supported by 111 Project (No. B17034) and the Innovative Research Team Development Program of the Ministry of Education of China (No. IRT17R83).

Data Availability Statement: The original contributions presented in the study are included in the article, further inquiries can be directed to the corresponding author.

Conflicts of Interest: The authors declare no conflicts of interest.

References

1. Qian, D.; Li, G.; Deng, J.; Wang, F. Effect of die structure on extrusion forming of thin-walled component with I-type longitudinal ribs. *Int. J. Adv. Manuf. Technol.* **2020**, *108*, 1959–1971. [[CrossRef](#)]
2. Zeng, X.; Fan, X.; Li, H.; Li, S. Flow forming process of thin-walled tubular parts with cross inner ribs. *Procedia Manuf.* **2018**, *15*, 1239–1246. [[CrossRef](#)]
3. Lei, Y.; Zhan, M.; Fan, X.; Zhang, A.; Niu, H.; Bai, D.; Gao, P.; Zheng, Z. A review on manufacturing technologies of thin-walled components with ribs. *J. Northwestern Polytech. Univ.* **2022**, *40*, 1–17. [[CrossRef](#)]
4. Hua, L.; Pan, L.B.; Lan, J. Researches on the ring stiffness condition in radial-axial ring rolling. *J. Mater. Process. Technol.* **2009**, *209*, 2570–2575. [[CrossRef](#)]
5. Kopp, R.; Böhlke, P. A New Rolling Process for Strips with a Defined Cross Section. *CIRP Ann.* **2003**, *52*, 197–200. [[CrossRef](#)]
6. Cleaver, C.J.; Lohmar, J.; Tamimi, S. Limits to making L-shape ring profiles without ring growth. *J. Mater. Process. Technol.* **2021**, *292*, 117062. [[CrossRef](#)]
7. Lohmar, J.; Cleaver, C.J.; Allwood, J.M. The influence of constraint rolls on temperature evolution and distribution in radial ring rolling. *J. Mater. Process. Technol.* **2020**, *282*, 116663. [[CrossRef](#)]
8. Li, X.; Guo, L.; Wang, F. On a plastic instability criterion for ultra-large radial-axial ring rolling process with four guide rolls. *Chin. J. Aeronaut.* **2021**, *35*, 391–406. [[CrossRef](#)]
9. Yeom, J.-T.; Kim, J.H.; Park, N.K.; Choi, S.-S.; Lee, C.S. Ring-rolling design for a large-scale ring product of Ti-6Al-4V alloy. *J. Mater. Process. Technol.* **2007**, *187*, 747–751. [[CrossRef](#)]
10. Liang, L.; Guo, L.; Liu, Z.H.; Wang, P.-P.; Zhang, H. On a precision forming criterion for groove-section profiled ring rolling process. *J. Mater. Process. Technol.* **2021**, *296*, 117207. [[CrossRef](#)]
11. Han, X.; Hua, L.; Lu, P.; Wei, F. An innovative radial envelope forming method for manufacturing thin-walled cylindrical ring with inner web ribs. *J. Mater. Process. Technol.* **2020**, *286*, 116836. [[CrossRef](#)]
12. Tian, D.; Han, X.; Hua, L.; Wang, X.; Chen, F. Constraining ring rolling of thin-walled conical rings with transverse ribs. *Int. J. Mech. Sci.* **2022**, *226*, 107394. [[CrossRef](#)]
13. Hua, L.; Deng, J.; Qian, D.; Lan, J.; Long, H. Modeling and application of ring stiffness condition for radial-axial ring rolling. *Int. J. Mach. Tools Manuf.* **2016**, *110*, 66–79. [[CrossRef](#)]
14. Tian, D.; Han, X.; Hua, L.; Hu, X. An innovative constraining ring rolling process for manufacturing conical rings with thin sterna and high ribs. *Chin. J. Aeronaut.* **2022**, *35*, 324–339. [[CrossRef](#)]
15. Zheng, Y. Multi-objective Optimization of Process Parameters of Aluminium Alloy Rib-web Forgings Based on Orthogonal Experiment. *Hot Work. Technol.* **2015**, *44*, 168–172.
16. Zhao, G.; Wright, E.D.; Grandhi, R.V. Preform Die Shape Design in Metal Forming Using an Optimization Method. *Int. J. Numer. Methods Eng.* **1997**, *40*, 1213–1230. [[CrossRef](#)]
17. Fourment, L.; Chenot, J.L. Optimal Design for Non-Steady-State Metal Forming Processes—I. Shape Optimization Method. *Int. J. Numer. Methods Eng.* **1996**, *39*, 33–50. [[CrossRef](#)]
18. Kusiak, J. A technique of tool-shape optimization in large scale problems of metal forming. *J. Mater. Process. Technol.* **1996**, *57*, 79–84. [[CrossRef](#)]

19. Montgomery, D.C. *Design and Analysis of Experiments*; John Wiley & Sons: Hoboken, NJ, USA, 2017.
20. Gheysarian, A.; Honarpisheh, M. Process Parameters Optimization of the Explosive-Welded Al/Cu Bimetal in the Incremental Sheet Metal Forming Process. *Iran. J. Sci. Technol. Trans. Mech. Eng.* **2018**, *43*, 945–956. [[CrossRef](#)]
21. Gulati, V.; Aryal, A.; Katyal, P.; Goswami, A. Process Parameters Optimization in Single Point Incremental Forming. *J. Inst. Eng. (India) Ser. C* **2015**, *97*, 185–193. [[CrossRef](#)]
22. Pan, Y.; Cai, G. Optimization of Processing Parameters of Aluminum Alloy Cylindrical Parts Based on Response Surface Method during Hydromechanical Deep Drawing. *Metals* **2023**, *13*, 1406. [[CrossRef](#)]
23. Li, W.; Zhang, Z.; Jia, H.; Ren, M. The Optimization of Welding Spots' Arrangement in A-Pillar Patchwork Blank Hot Stamping. *Metals* **2023**, *13*, 1409. [[CrossRef](#)]
24. Hu, J.; Wen, T.; Zhang, M.; Zhang, Z. Optimization on rolling process parameters for rib stiffened plates based on respond surface method. *Forg. Stamp. Technol.* **2019**, *44*, 35–40.
25. Hu, Z.; Wei, Z.; Sun, H.; Yang, J.; Wei, L. Optimization of Metal Rolling Control Using Soft Computing Approaches: A Review. *Arch. Comput. Methods Eng.* **2019**, *28*, 405–421. [[CrossRef](#)]
26. Feng, W.; Hua, L. Multi-objective optimization of process parameters for the helical gear precision forging by using Taguchi method. *J. Mech. Sci. Technol.* **2011**, *25*, 1519–1527.
27. Feng, W.; Hua, L. Process Parameters Optimisation for Helical Gears Precision Forging with Damage Minimization. In Proceedings of the 2010 International Conference on Digital Manufacturing & Automation, Changsha, China, 18–20 December 2010; pp. 117–120.
28. Anupama Francy, K.; Sai Sudheer, S.V.; Naga Krishna, N.; Gopalakrishnaih, P. Optimization of input process parameters for Al 2024 alloy in cold extrusion process. *Mater. Today Proc.* **2023**. [[CrossRef](#)]
29. Li, H.; Chang, C.; Huang, Y.; Fu, R.; Shao, H. Optimization of numerical parameters and microstructure evolution on 2195 Al–Li alloy extrusion process. *J. Mater. Res. Technol.* **2023**, *26*, 7694–7706. [[CrossRef](#)]
30. Luo, W.; Tang, L.; Guo, F. Mold design and forming process parameters optimization for passenger vehicle front wing plate. *J. Mech. Sci. Technol.* **2022**, *36*, 187–196. [[CrossRef](#)]
31. Hosseini, S.H.; Sedighi, M.; Mosayebnezhad, J. Numerical and experimental investigation of central cavity formation in aluminum during forward extrusion process. *J. Mech. Sci. Technol.* **2016**, *30*, 1951–1956. [[CrossRef](#)]

Disclaimer/Publisher's Note: The statements, opinions and data contained in all publications are solely those of the individual author(s) and contributor(s) and not of MDPI and/or the editor(s). MDPI and/or the editor(s) disclaim responsibility for any injury to people or property resulting from any ideas, methods, instructions or products referred to in the content.